Theor. Appl. Climatol. 90, 49–63 (2007)
DOI 10.1007/s00704-006-0274-0
Printed in The Netherlands

Theoretical and Applied Climatology

Research and Development Centre, Snow and Avalanche Study Establishment, Him Parisar, Chandigarh, India

The transport of momentum, sensible heat, potential energy and moisture over the western Himalayas during the winter season

A. P. Dimri

With 19 Figures

Received September 28, 2005; revised February 8, 2006; accepted August 14, 2006
Published online February 21, 2007

Summary

The western Himalayas receive higher precipitation than the eastern Himalayas during the winter season (December–March). This differential pattern of winter precipitation over the Himalayas can be attributed to topography and to a higher frequency of disturbances over the western Himalayas, which result in variations in the circulation features. These circulation features, in turn, result in variations in the meridional transport of heat, momentum, potential energy, and moisture across the Himalayas due to mean and eddy motion.

Significant meridional transport due to mean motion takes place in the upper troposphere at 300 hPa and 200 hPa. Transport east of 100° E dominates the transport over the western Himalayas. The eddy transport of heat, momentum, and potential energy is considerably smaller than that due to mean motion. Eddy transport magnitudes are smaller up to 500 hPa and increase rapidly aloft to 300 hPa and 200 hPa. Eddy transport over the western Himalayas is greater than over the eastern Himalayas.

1. Introduction

Western disturbances (WDs) are important synoptic weather systems that move west to east across the Himalayas and bring precipitation in the form of snow or rain over the region during the winter months from December through March (DJFM). WDs are low-pressure synoptic weather systems that originate over the Mediterranean Sea or mid-Atlantic Ocean and travel eastward over Iran, Afghanistan, Pakistan, and northwest India. These weather systems follow their southernmost tracks during winter and pass over northwest India. WDs may arise from eastward-moving extratropical cyclones that penetrate southward. Monthly (December–March) and seasonal (DJFM) averaged precipitation amounts drawn from forty years (1958–1997) of the National Center for Environmental Prediction–National Center for Atmospheric Research, US (NCEP–NCAR; hereafter NCEP) reanalysis data are presented in Figs. 1 and 2, respectively. Precipitation in the western Himalayan region varies substantially from season to season and is highest in winter. This differential pattern can be attributed not only to the topography but to the higher frequency of WDs over the western Himalayas. In addition, atmospheric circulation patterns and the resulting precipitation patterns are influenced by land surface properties such as snow cover, vegetation cover, albedo, and soil moisture.

A better understanding of the mechanisms involved in the mean evolution of these sys-

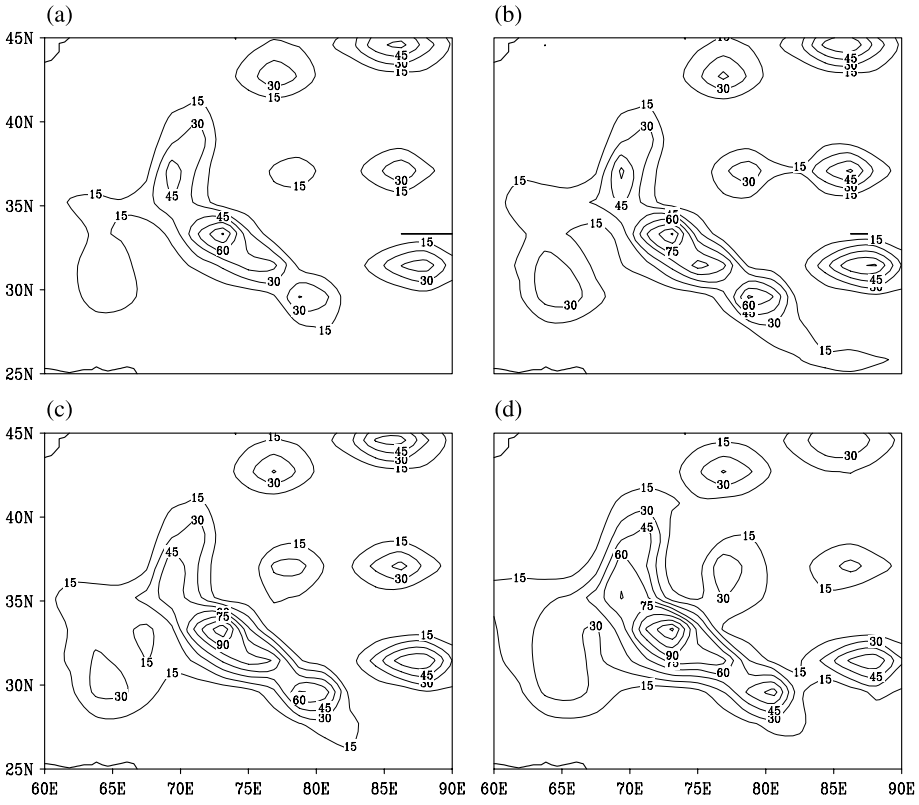

Fig. 1. Monthly averaged precipitation for (**a**) December, (**b**) January (**c**) February and (**d**) March, 1958–1997 (units: cm)

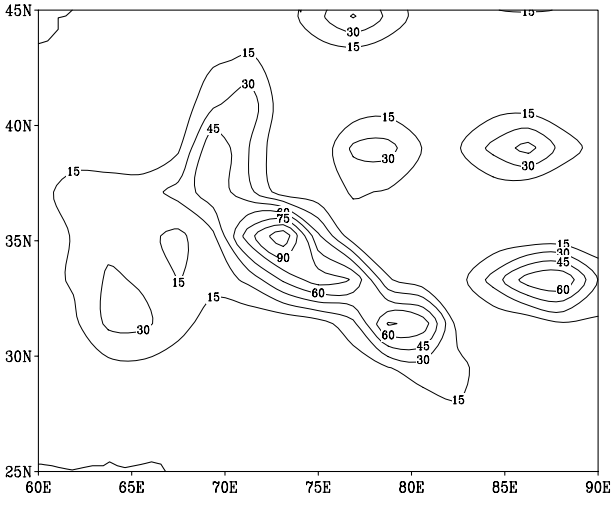

Fig. 2. Seasonal (DJFM) averaged precipitation for DJFM, 1958–1997 (units: cm)

tems and their spatial and temporal variability can be achieved through the use of diagnostic studies based on observational data sets and numerical models. It is therefore vital to better predict and simulate the mechanism on various time scales (Kung and Smith, 1974; Pearce, 1979; Krishnamurti et al., 1998). The study of mean diagnostic features in times of surplus and deficient seasonal precipitation during winter circulation over the western Himalayas will contribute to the better understanding of these systems (Dimri, 2005, 2006). Several studies (Joseph, 1975; Krueger and Winston, 1975; Kanamitsu and Krishnamurti, 1978) have been carried out to analyze the contrasting circulation features and the energetics of normal and deficient monsoon seasons. Krishnamurti et al. (1989, 1990) came out with a detailed comparison of the evolution of parameters such as outgoing longwave radiation, sea surface temperature, steam function anomalies, divergent circulation, and precipitation patterns to identity differences between dry (1987) and wet (1988) monsoon seasons over India.

Although a number of studies have reported on the diagnostic aspects of the atmosphere, few studies have focused on wintertime circulation patterns over the western Himalayas. Difficult topography (Fig. 3) makes most of the region inaccessible for routine meteorological and climatological observations and data are scarce. The recent efforts of NCEP in generating reanalysis data to study climate trends are laudable. Various studies (Chen et al., 1996; Annamalai et al., 1999; Ramesh Kumar et al., 1999; Sperber et al., 2000) making use of NCEP reanalysis confirm the use-

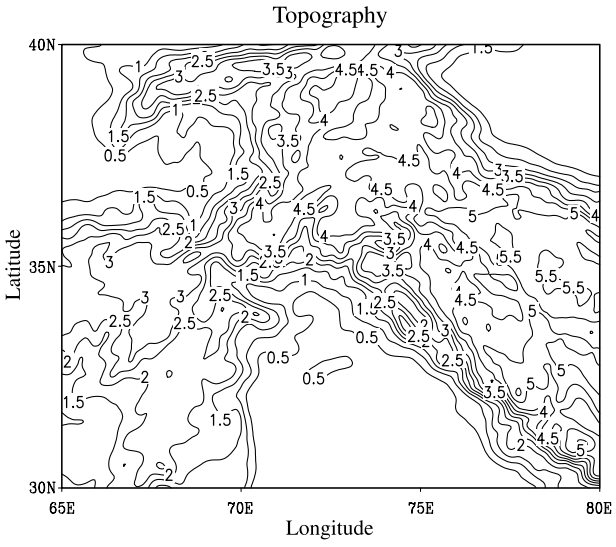

Fig. 3. Schematic representation of geography and topography (m) of the region under study

fulness of these data sets. The availability of globally analyzed upper air meteorological fields from NCEP enhances the scope of study of these mechanisms over the data-sparse Himalayan region.

The NCEP data set has been used to study large-scale meridional transport terms across the Himalayan region during DJFM. With the above objectives in mind, the present study examines momentum, sensible heat, potential energy and moisture terms during DJFM for the period of 1958–1997. The data and scheme of analysis are briefly discussed in Sect. 2, followed by results and discussion in Sect. 3. A summary of the results appears in Sect. 4.

2. Data and methodology

The NCEP reanalysis project (Kalnay et al., 1996) used an advanced global data assimilation systems (GDAS) that utilizes data from diverse sources. The use of observations in conjunction with a state-of-the-art assimilation system has enhanced the reliability of NCEP products. In the present study, the database comprises daily upper air fields from the NCEP reanalysis for the 40-year period from 1958 to 1997. This reanalysis provides a consistent and reliable data set for examining the momentum, heat, potential energy and moisture terms over the Himalayas. The data used comprises daily averaged NCEP reanalysis fields of zonal wind (u), meridional

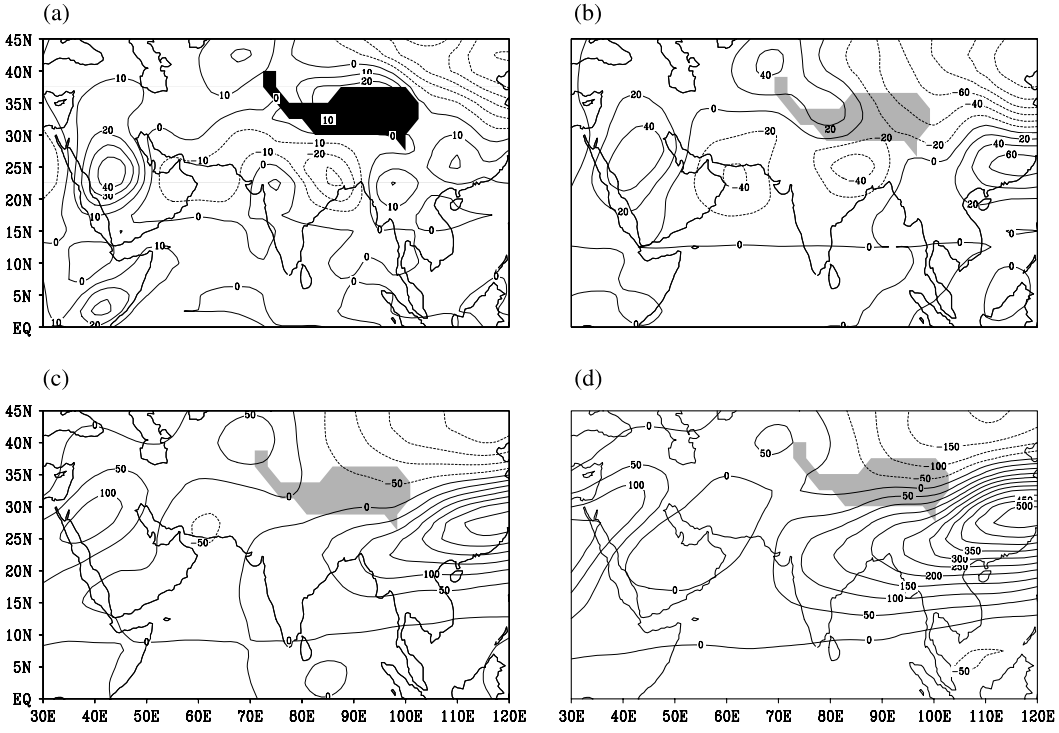

Fig. 4. Geographical distribution of vertically integrated meridional transport of momentum due to mean motion for DJFM, 1958–1997 (units: $m^2 s^{-2}$) (**a**) 700 hPa (**b**) 500 hPa (**c**) 300 hPa (**d**) 200 hPa (Black shading represents topography at 700 hPa, whereas shaded portion at 500, 300 and 200 hPa is projection of 700 hPa topography)

wind (v), omega (w), temperature (T), geopotential height (Z), and specific humidity (q) at 0000 UTC for DJFM. The region of study extends from 15° S to 45° N and 30° E to 120° E at the 1000, 850, 700, 500, 300, 200 and 100 hPa levels.

2.1 Transient and stationary eddies

Understanding of the circulation characteristics of the atmosphere requires the study of statistics of various orders of important meteorological variables. Following Starr and White (1951) these statistics can be defined in both space and time and in a mixed space-time domain.

The time average of a quantity A for a specific time interval T can be represented as

$$\bar{A} = \frac{1}{T}\int_0^T A\,dt. \tag{1}$$

If the deviation from the average is A' then

$$A = \bar{A} + A' \tag{2}$$

where $\bar{A}' = 0$.

Furthermore, the average product of two quantities, A and B, is given by

$$\overline{AB} = \bar{A}\bar{B} + \overline{A'B'}. \tag{3}$$

First Eq. (3) is examined for momentum and heat terms. Thus putting $A = u$, and $B = v$, where u and v are the zonal and meridional components of wind,

$$\overline{uv} = \bar{u}\bar{v} + \overline{u'v'}. \tag{4}$$

The first term on the right represents meridional transport of u-momentum due to mean motion or flux of relative momentum due to mean motion; the second term represents the meridional transport of u-momentum due to transient eddies.

Similarly,

$$\overline{vT} = \bar{v}\bar{T} + \overline{v'T'}. \tag{5}$$

The first term on the right indicates the meridional transport of sensible heat due to mean motion and the second term represents the meridional transport of sensible heat due to transient eddies. Similar computations were made with meteorological variables for the remaining flux terms.

Using daily averaged values of zonal wind (u), meridional wind (v), omega (w), temperature (T), geopotential height (Z), and specific humidity (q) at 0000 UTC at grid points for the 40 years (1958–1997), the following means, variances, covariances for DJFM, and seasons were evaluated over the study region:

$\bar{u}$	$\bar{v}$	$\bar{w}$	$\bar{T}$	$\bar{Z}$	$\bar{q}$
$\overline{u'u'}$	$\overline{u'v'}$	$\overline{u'w'}$	$\overline{u'T'}$	$\overline{u'Z'}$	$\overline{u'q'}$
–	$\overline{v'v'}$	$\overline{v'w'}$	$\overline{v'T'}$	$\overline{v'Z'}$	$\overline{v'q'}$
–	–	$\overline{w'w'}$	$\overline{w'T'}$	$\overline{w'Z'}$	$\overline{w'q'}$
–	–	–	$\overline{T'T'}$	$\overline{T'Z'}$	$\overline{T'q'}$
–	–	–	–	$\overline{Z'Z'}$	$\overline{Z'q'}$
–	–	–	–	–	$\overline{q'q'}$

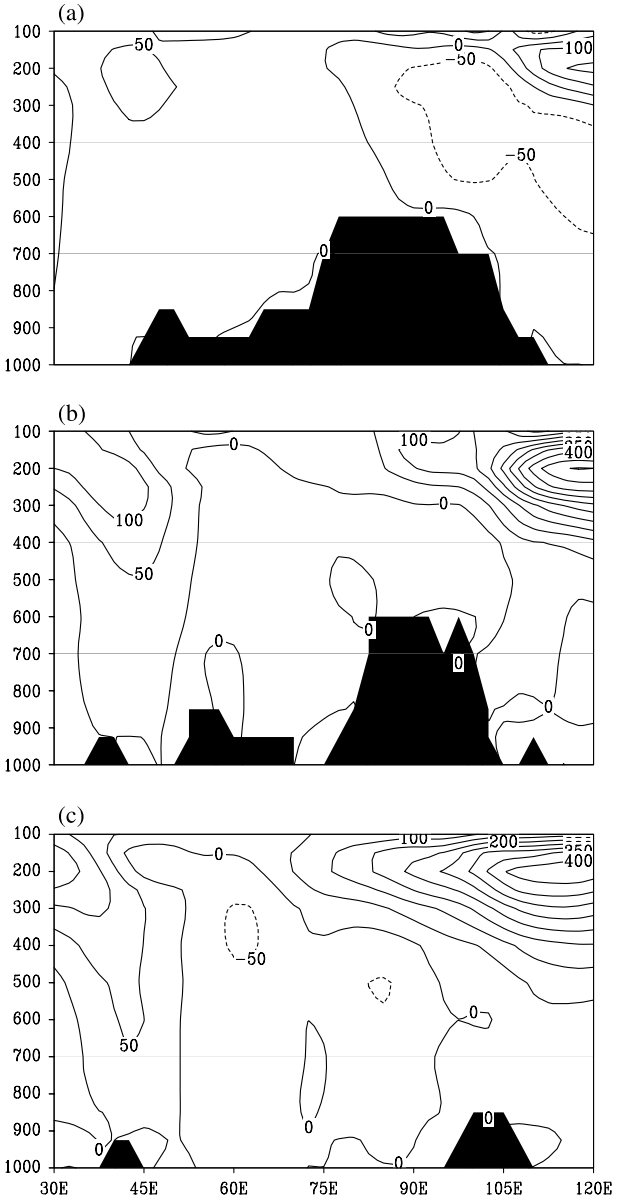

Fig. 5. Sectorial mean pressure longitude cross section of meridional transport of momentum due to mean motion for DJFM, 1958–1997 (units: $m^2\,s^{-2}$) (**a**) 35° N (**b**) 30° N (**c**) 25° N (Black shading represents topography)

Since meridional transport is more important for large-scale processes, results pertaining to meridional transport due to mean and eddy motion with respect to momentum, sensible heat, potential energy, and specific humidity are discussed and elaborated in the next section of this study.

3. Results and discussion

3.1 Meridional transport of u-momentum due to

3.1.1 Mean motion ($\bar{u}\bar{v}$)

The geographical distribution of vertically integrated meridional transport of momentum due to mean motion for DJFM 1958–1997 is presented in Fig. 4. The seasonal meridional transport of momentum shows the dominant transport features due to mean motion at 700, 500, 300, and 200 hPa. Northward transport of momentum due to mean motion across the Himalayan region extending from 50° E to 90° E and 25° N to 40° N is found up to 500 hPa (Fig. 4b). The magnitude varies between 10 and 20 $m^2 s^{-2}$. To the east of this, strong southward transport of momentum can be seen over the northern part of southeast China, whereas over the southern part of southeast China, strong northward transport of momentum is prevalent. Two relatively significant southward transports of momentum can be seen over the head of the Bay of Bengal and the Arabian Sea at 500 hPa (Fig. 4b). At 300 hPa and 200 hPa (Fig. 4c, d), transport is comparatively weak and is toward the north across the western Himalayas; it increases towards the south of China. A strong centre of northward transport of momentum of the magnitude of 500 $m^2 s^{-2}$ can be observed over southeast China (Fig. 4d). Since the Himalayan ranges are oriented northwest to southeast, the orientation and topography of the Himalayan ranges could lead to southerly transport of momentum up to about 500 hPa. At higher levels, the distribution of transport of momentum gains could be due to the subtropical westerly jet stream which takes a north-northeasterly course and strengthens east of 90° E. Northeast China experiences northward transport of momentum due to the northwest–southeast orientation of the polar jet. We have found that the strongest subtropical jet stream in this region is over northeast China and Japan.

A sectorial mean pressure longitude cross-section of meridional transport of momentum due to mean motion for DJFM 1958–1997 at 25° N,

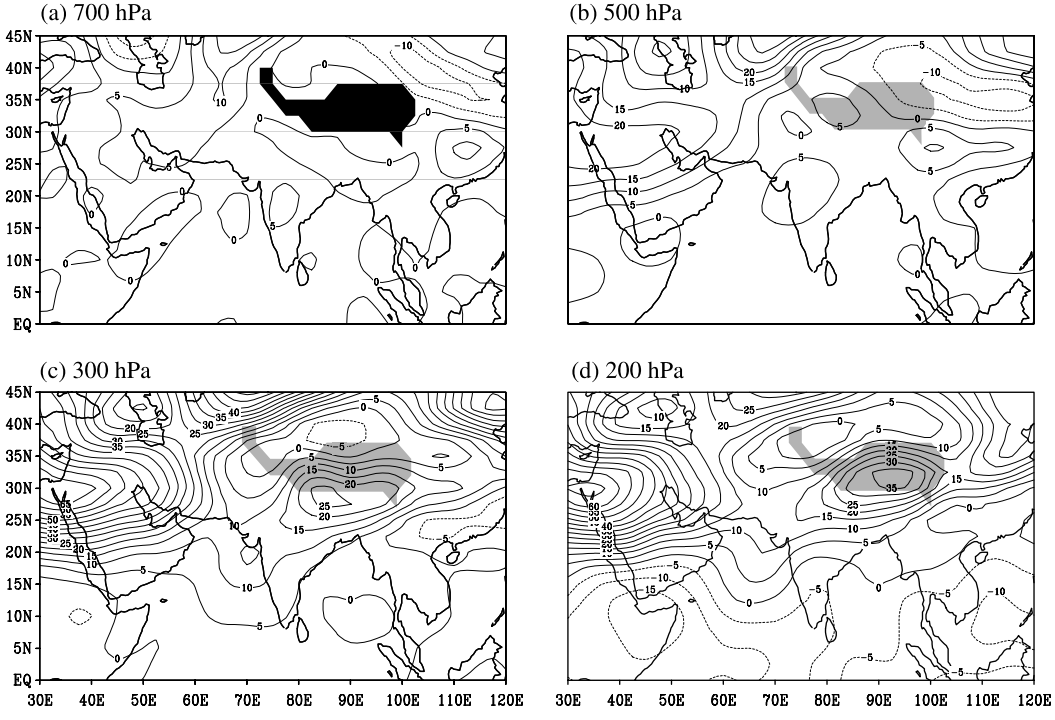

Fig. 6. Same as Fig. 4, but for meridional transport of momentum due to eddy motion (units: $m^2 s^{-2}$)

30° N and 35° N is shown in Fig. 5. Strong northward transports can be observed in the vicinity of the subtropical jet stream, particularly at the western and eastern ends of the Himalayas. The maximum meridional transport of momentum due to mean motion is located over southeast China, where the subtropical westerly jet gains a considerably higher speed. To the north of the Himalayas, from 50° E to 90° E, the magnitude of meridional transport of momentum due to mean motion is significantly smaller, as indicated by the cross-section at 35° N and 30° N (Fig. 5a, b). Across the Himalayas, meridional transport of momentum is at a minimum, whereas to the west and east of the Himalayas, momentum transport due to mean motion is northward and higher. Two maxima of momentum transport are seen at 200 hPa at 35° E and 115° E; the magnitude of which decreases northward from 25° N to 35° N.

3.1.2 Eddy motion ($\overline{u'v'}$)

Vertically integrated meridional transport of momentum due to eddy motion at the 700, 500, 300, and 200 hPa pressure levels is shown in Fig. 6. Small magnitudes of transport of momentum are observed up to 500 hPa across the Himalayas; however, at 300 and 200 hPa (Fig. 6c, d), the magnitude increases reaching up to $30\,m^2s^{-2}$ over the western end of the Himalayas. This magnitude is considerably smaller than that due to mean motion as shown in Fig. 4. This eddy transport maxima is due to fluctuations in the anticyclonic cell located at 300 hPa and 200 hPa over the Bay of Bengal during the winter (DJFM). Towards the west of the Bay of Bengal, the northward transport of eddy momentum reaches a maximum of $65\,m^2\,s^{-2}$ over the Red Sea. This magnitude is comparable with the mean transport and is due to a) troughs in the upper tropospheric westerlies that follow a north-northeasterly course over this region and b) fluctuations in the subtropical westerly jet stream. Synoptic disturbances in the Arabian Sea, Bay of Bengal and equatorial Indian Ocean could also generate fluctuations in the lower and upper tropospheric flow. The eddy transport of momentum over the western end of the Himalayas is higher compared to the eastern end in the lower and middle troposphere, whereas the reverse is seen aloft. Moreover, mean eddy transport of momentum is always northward north of 15° N.

A sectorial mean pressure longitude cross-section of meridional transport of momentum due to eddy motion at 25° N, 30° N and 35° N, from 1000 to 100 hPa, is shown in Fig. 7. The vertical cross-section at 30° N (Fig. 7b) shows strong maxima of northward transport along the longitude of 35° E and 90° E between 300 and 200 hPa, whereas the magnitude of momentum transport due to eddy motion decreases north and south of 30° N. Again, this maximum at ∼300 hPa is due to fluctuations in the anticyclo-

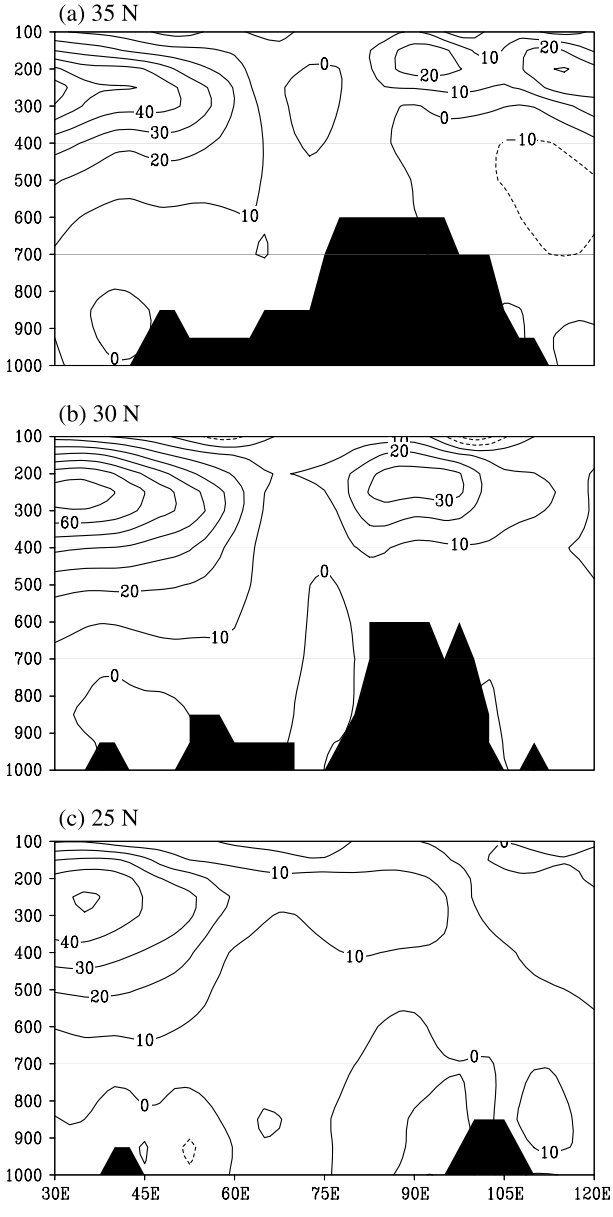

Fig. 7. Same as Fig. 5, but for meridional transport of momentum due to eddy motion (units: $m^2\,s^{-2}$)

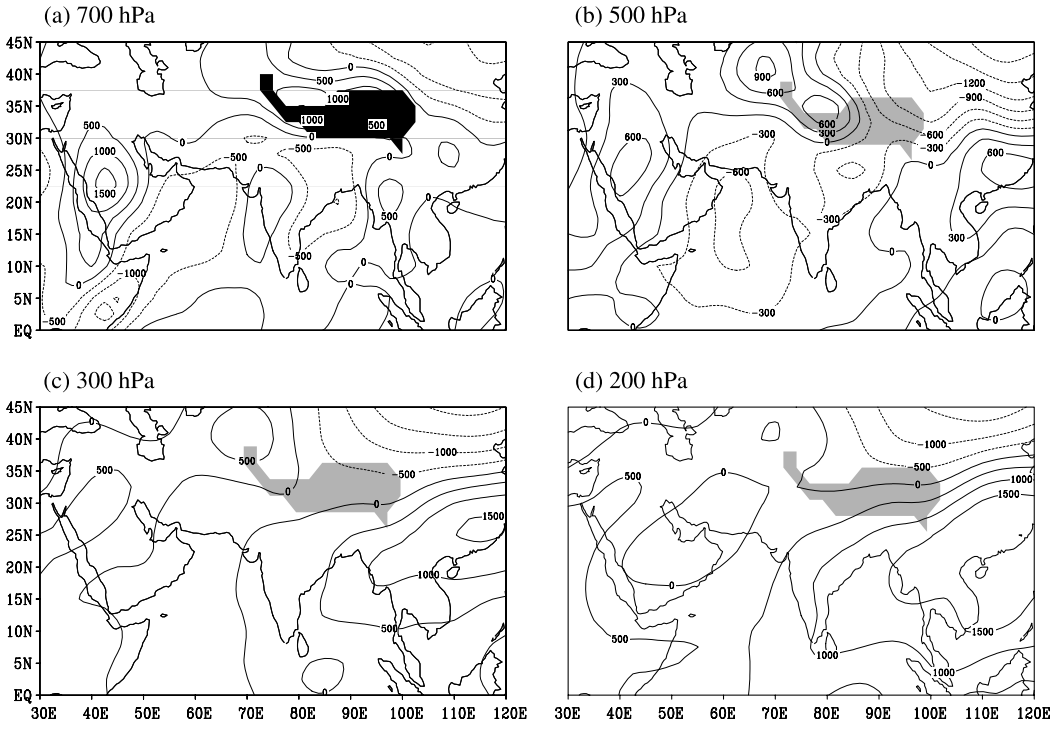

Fig. 8. Same as Fig. 4, but for meridional transport of sensible heat due to mean motion (units: $\mathrm{K\,ms^{-1}}$)

nic cells located at this level over the Bay of Bengal during the winter. This can be attributed to the fact that during the passage of WDs, the complex topography of the western Himalayas moderately modifies the westerly flow around 30° N by generating more eddy transport of momentum. Strong northward transport of momentum is prevalent at this latitude (Fig. 7).

3.2 Meridional transport of sensible heat due to

3.2.1 Mean motion ($\bar{v}\bar{T}$)

The geographical distribution of vertically integrated meridional transport of sensible heat by mean motion at 0000 UTC at 700, 500, 300 and 200 hPa is shown in Fig. 8. The pattern at 700 hPa, Fig. 8a, shows the southward transport of sensible heat over peninsular India, except over parts of Gujarat and Maharastra. The magnitude of which varies between 300 and 900 $\mathrm{K\,ms^{-1}}$. Southward transport would imply colder air travelling southwards over the Indian Peninsula if there is northward transport of heat. The desert conditions of northwest India probably account for such behaviour. The magnitude of which varies between 1000 and 1500 $\mathrm{K\,ms^{-1}}$. At 500 hPa, Fig. 8b, northward transport of sensible heat is seen along the western and central Himalayas. The Tibetan region also contributes to the northward transport of sensible heat. At 300 and 200 hPa, Fig. 8c, d, the heat transport across the western Himalayas is negligible, but across the eastern Himalayas and further eastwards, it gains strength and is directed northwards. The production of more sensible heat gives rise to the vertical motion under which moisture is lifted and after undergoing thermodynamical processes precipitation processes are initiated which ultimately yields large amounts of precipitation.

The sectorial mean pressure longitude cross-section of meridional transport of sensible heat due to mean motion at 25° N, 30° N and 35° N is shown in Fig. 9. The cross-section at 25° N, Fig. 9c, clearly shows the southward heat transport over the region between 50° E and 95° E from surface to 300 hPa. However, east of 95° E and west of 50° E, heat transport is northwards and is confined to the lower and upper troposphere. The magnitude of which varies between 1250 and 1750 $\mathrm{K\,ms^{-1}}$. At 30° N, Fig. 9b, the latitude crossing the Himalayas, magnitudes are smaller and negative, but to the west and east of the Himalayas, the heat transport is northwards

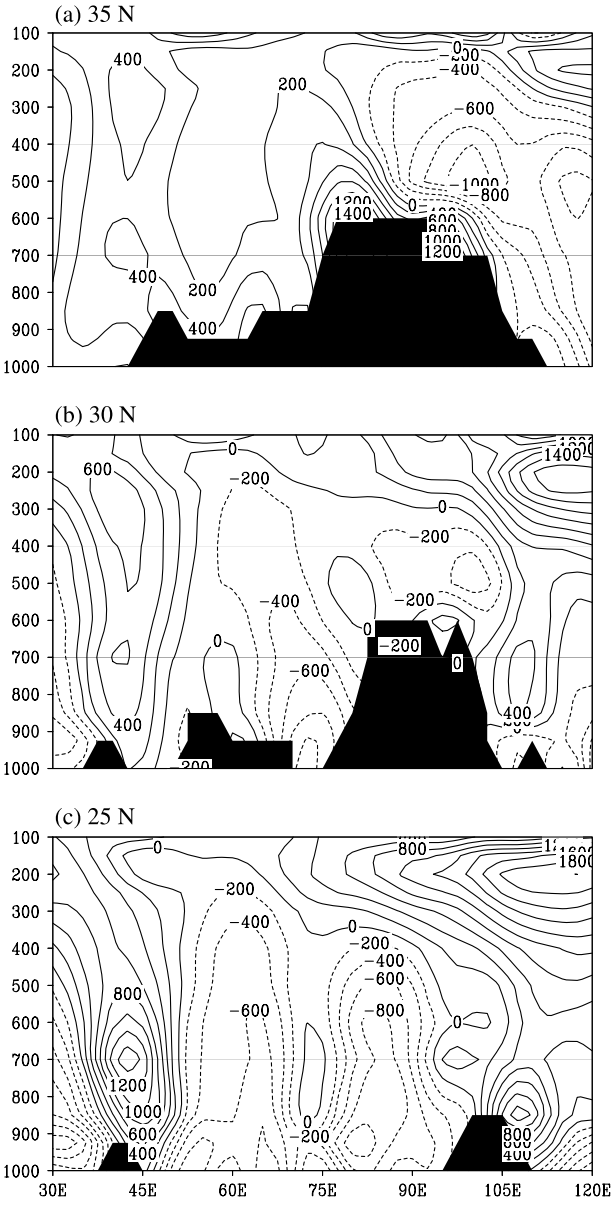

Fig. 9. Same as Fig. 5, but for meridional transport of sensible heat due to mean motion (units: $\mathrm{K\,ms^{-1}}$)

and varies between 500 and 1500 $\mathrm{K\,ms^{-1}}$ at and around 200 hPa. At 35° N, west of 95° E experiences northward transport whereas east of 95° E experiences the southward transport of sensible heat. In the jet stream region, between 25° N and 30° N and east of 90° E, the maximum northward transport of heat due to mean motion takes place. Due to the heterogeneity of the topography and landuse, destruction/production of sensible heat over the western Himalayan region plays a significant role, governing the intensity of precipitation over the region.

3.2.2 Eddy motion ($\overline{v'T'}$)

Vertically integrated meridional transport of sensible heat due to eddy motion is shown in Fig. 10. It is clear that transport due to eddy motion is very small compared to the mean motion. The direction of transport, by eddy motion remains the same, i.e. southwards over the Indian peninsula up to 500 hPa, whereas above 500 hPa northward transport of sensible heat is observed. The maximum northward transport of sensible heat due to eddy motion takes place between 30° E to 40° E and 110° E to 120° E in the upper troposphere at 300 hPa. Eddy transport at the western end of the Himalayas is higher as compared to the eastern end. However, at 300 hPa a weak cell of southward transport of sensible heat due to eddy motion is seen over the Himalayan region. Strong maximum northward transport of sensible heat due to eddy motion is seen over Saudi Arabia and north of northeast China. At 200 hPa, strong northward transport of sensible heat due to eddy motion is seen along the entire region. Overall, distribution patterns shown by eddy motion are opposite to that observed due to mean motion. Eddy flow is more prominent over the western Himalayas than over the eastern Himalayas during the passage/presence of the WDs because more sensible heat is generated at the time of passage/presence of the WD, which very rarely affects the eastern Himalayas during winter.

Sectorial mean pressure longitude cross-section of meridional transport of sensible heat due to eddy motion during DJFM, 1958–1997 at 25° N, 30° N and 35° N is shown in Fig. 11. Southward transport of sensible heat due to eddy motion is seen in the middle troposphere at 75° E at all latitudes, whereas a strong northward transport of sensible heat due to eddy motion is prevalent from the surface to the upper troposphere between 105° E and 120° E. In addition, the strong northward transport of sensible heat due to eddy motion is observed in the lower troposphere at and around 50° E at all latitudes. A similar strong maximum is observed at and around 300 hPa. Figure 11 shows the clear effect of the Himalayan range on the eddy transport of sensible heat over the study region. Due to the orientation of the western Himalayas more disturbances are formed on the windward side of the mountain due to topographic/orographic and mechanical/thermodynamical forcings.

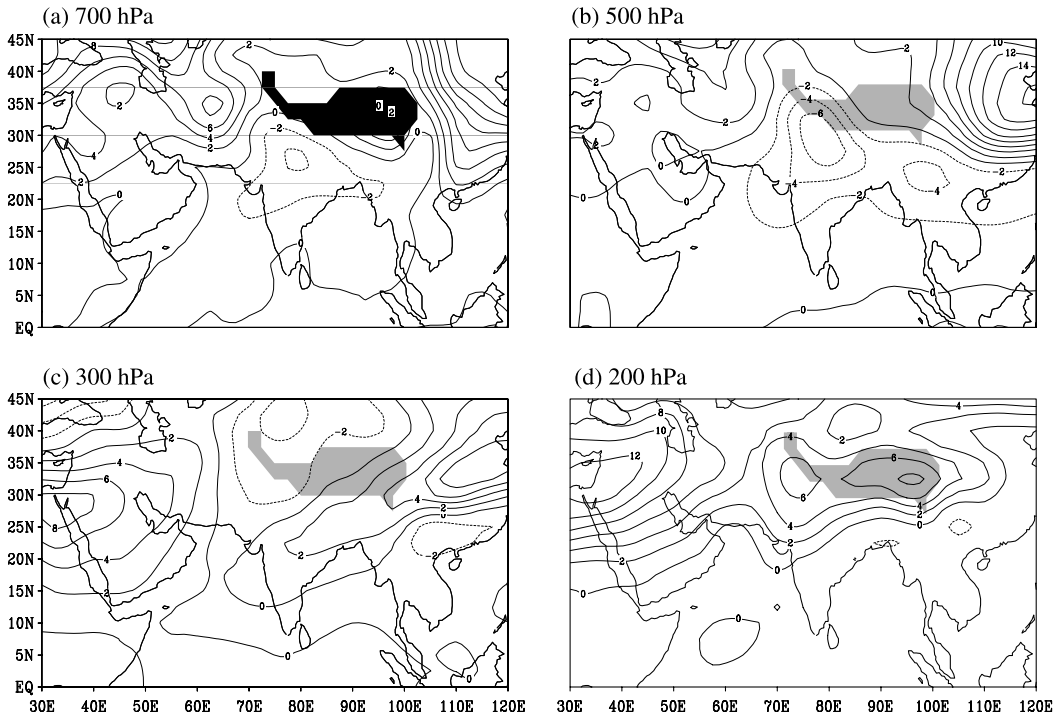

Fig. 10. Same as Fig. 4, but for meridional transport of sensible heat due to eddy motion (units: K ms^{-1})

3.3 Meridional transport of potential energy due to

3.3.1 Mean motion ($\bar{v}\,\bar{z}$)

The geographical distribution of vertically integrated meridional transport of potential energy due to mean motion for DJFM, 1958–1997 at 0000 UTC at 700, 500, 300 and 200 hPa is shown in Fig. 12. This pattern resembles the meridional transport of sensible heat shown in Fig. 8. At 700 hPa, potential energy transport across the Himalayas is very small, while at the eastern and the western ends potential energy is transported northwards. At 500 hPa, Fig. 12b, the strong northward transport of potential energy due to mean motion is prevalent along the Himalayas. Whereas over the Arabian Sea, Indian Peninsula and north China, the strong southward transport of potential energy due to mean motion is observed. In contrast, Saudi Arabia and south of southeast China experience northward transport. A similar distribution of transport of potential energy due to mean motion is seen at 300 hPa except over the Indian Peninsula where the northward transport of potential energy is prevalent. An increase in the magnitude of transport of potential energy is also seen. Strong northward transport of potential energy is seen across the entire region at 200 hPa except over north China and Saudi Arabia where the southern transport of potential energy due to mean motion is prevalent. Convergence of potential energy over the region generates more circulation which ultimately modulate the WDs embedded in the westerlies and hence generate more precipitation, whereas the reverse is the case during the divergence of potential energy.

A sectorial mean pressure longitude cross-section of meridional transport of potential energy along 25° N, 30° N and 35° N is shown in Fig. 13. Sectorial distribution shows strong northward transport of potential energy due to mean motion at lower latitudes around 200 hPa, between 105° E and 120 °E. This feature becomes weaker towards higher latitudes. At 35° N and 90° E, a strong cell of northward transport of potential energy is seen in the middle troposphere, whereas at lower latitudes few cells of southward transport of potential energy due to mean motion are seen. In addition, a strong cell of northward transport of potential energy due to mean motion from the surface to 100 hPa is seen at and around

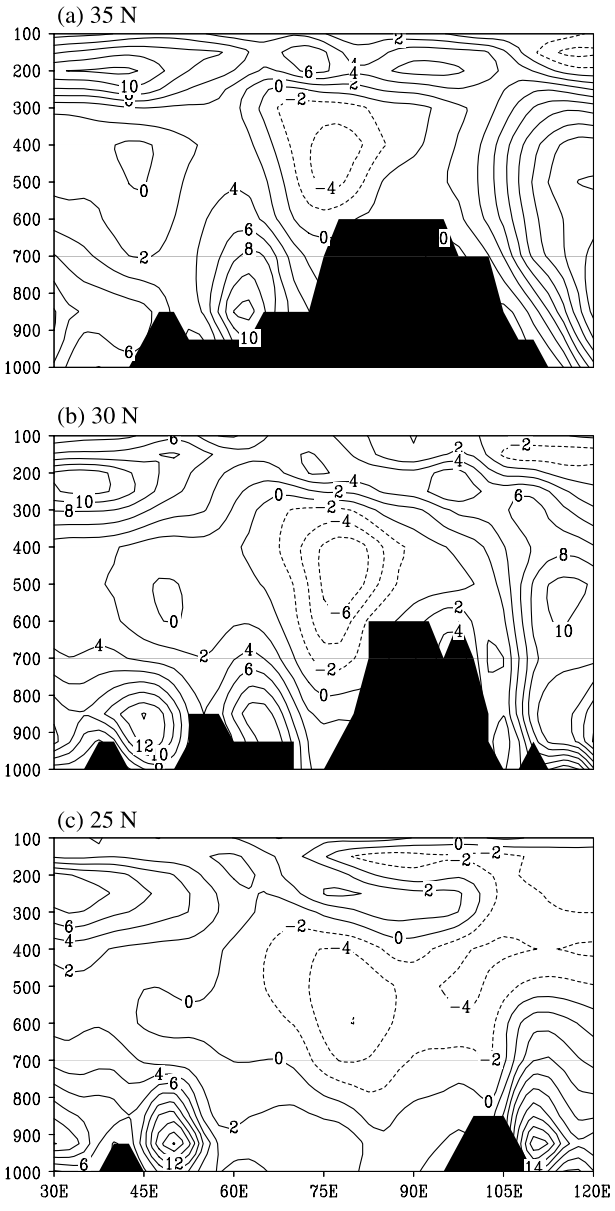

Fig. 11. Same as Fig. 5, but for meridional transport of sensible heat due to eddy motion (units: K ms^{-1})

30° E to 45° E. The effect of the Himalayan topography is clearly seen on the distribution of potential energy due to mean motion.

3.3.2 Eddy motion ($\overline{v'z'}$)

The distribution of vertically integrated seasonal meridional transport of potential energy due to eddy motion is shown in Fig. 14. Although eddy transport of potential energy is considerably smaller than mean motion, constant southward transport from 700 to 200 hPa from the Arabian Sea to north of the Himalayas is observed. In addition to this, a strong gradient of northward transport of potential energy due to eddy motion is seen at and around 115° E and 40° N. Furthermore, significant northward transport of potential energy due to eddy motion is seen from 500 hPa to 200 hPa at and around 30° N, which gradually becomes stronger from the lower to upper troposphere. Over northwest Africa and Saudi Arabia, southward transport of potential energy due to eddy motion is prevalent and reaches a maximum in the upper troposphere. This northward transport of potential energy over the Indian subcontinent leads to the occurrence of most of the precipitation by amassing moisture from the Arabian Sea over the Indian Himalayan region. This northward transport of potential energy is associated with WDs embedded in the westerly flow and hence yields large amount of precipitation.

The sectorial mean pressure longitude cross-section of potential energy due to eddy motion at 25° N, 30° N and 35° N is shown in Fig. 15. The increase in the southward transport of potential energy due to eddy motion is seen over the Himalayan region at 35° E and 75° E, as we move from lower latitudes to higher latitudes at and around 300 hPa. The strongest maxima are located at and around 300 hPa at all the three latitudes. The gradient of eddy transport of potential energy shows that most of the transport is at and around the Himalayan region, which emphasizes the fact that the local topography plays a very significant role in modifying the winter weather. This addition of potential energy with existing westerly flow embedded with WDs contributes to the enhancement of precipitation over the region of study.

3.4 Meridional transport of moisture due to

3.4.1 Mean motion ($\bar{v}\bar{q}$)

The geographical distribution of vertically integrated seasonal transport of moisture due to mean motion at the pressure levels of 700 hPa, 500 hPa and 300 hPa is shown in Fig. 16. Northward transport of moisture is seen over the Himalayan region at 700 hPa which decreases from the lower (700 hPa) to upper troposphere (300 hPa). In addition, northward transport of moisture is seen along the west coast of India and the reverse

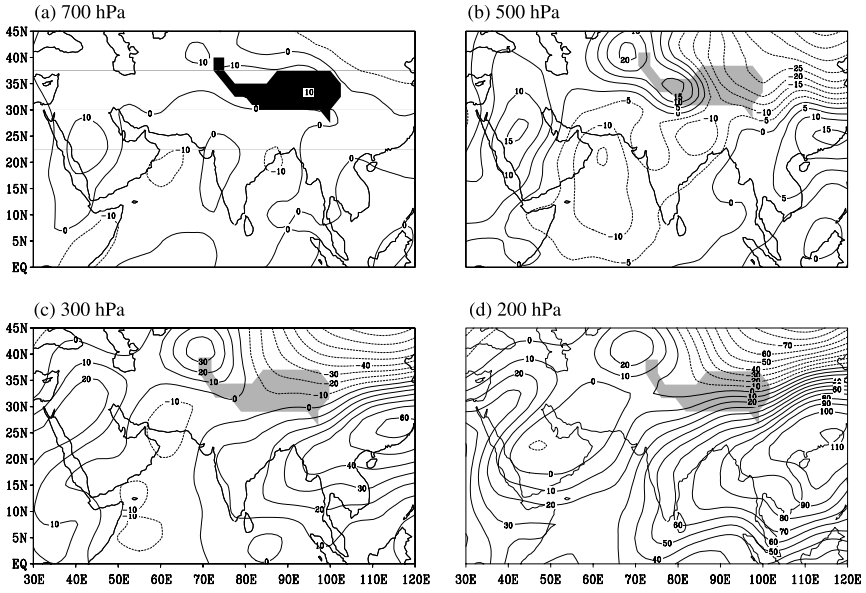

Fig. 12. Same as Fig. 4, but for meridional transport of potential energy ($\times 10^{-3}$) due to mean motion (units: $m^2\,s^{-1}$)

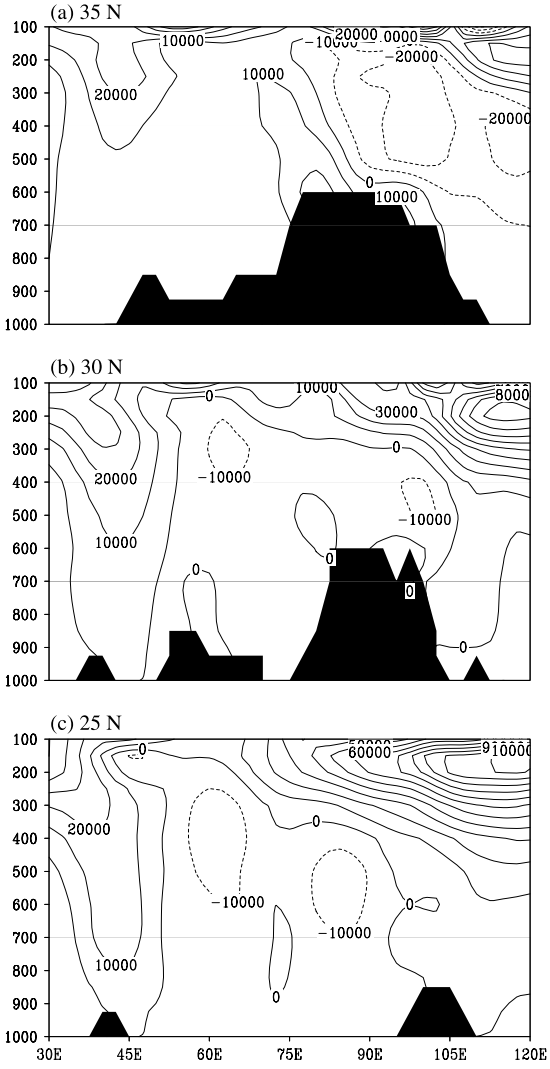

along the east coast at 700 hPa. Aloft at 500 hPa, across the Indian peninsula, the southwest transport of moisture is prevalent, whereas at 300 hPa northward transport of moisture is seen which gets stronger towards the south of China. Over North China, the northward transport of moisture is observed at 700 hPa, which is reversed at 500 hPa. Strong southward transport of moisture is observed over the Red Sea and Saudi Arabia at 700 hPa, which decreases aloft at 500 hPa and 300 hPa. The Arabian Sea may be the source region if, at lower levels (<700 hPa), moisture converges northwards and is lifted.

Sectorial mean pressure longitude cross-section of meridional transport of moisture due to mean motion at 25° N, 30° N and 35° N is shown in Fig. 17. This reveals the very interesting distribution of moisture transport. Most of the transport is confined within the lower troposphere. At 25° N, the strong northward transport of moisture due to mean motion is seen at 45° E and 105° E. Apart from this, across most of the region, southward transport of moisture remains prevalent in the lower troposphere. Overall, it is observed that moisture transport by mean motion at 500 hPa and aloft is negligible over the study region. At 35° N (Fig. 17a) the northward transport of mois-

Fig. 13. Same as Fig. 5, but for meridional transport of potential energy due to mean motion (units: $m^2\,s^{-1}$)

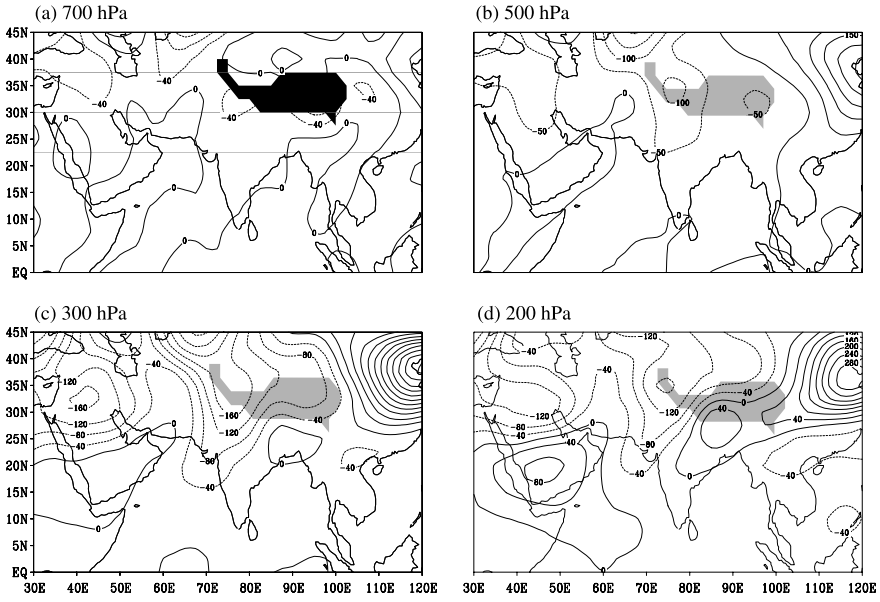

Fig. 14. Same as Fig. 4, but for meridional transport of potential energy due to eddy motion (units: $m^2\,s^{-1}$)

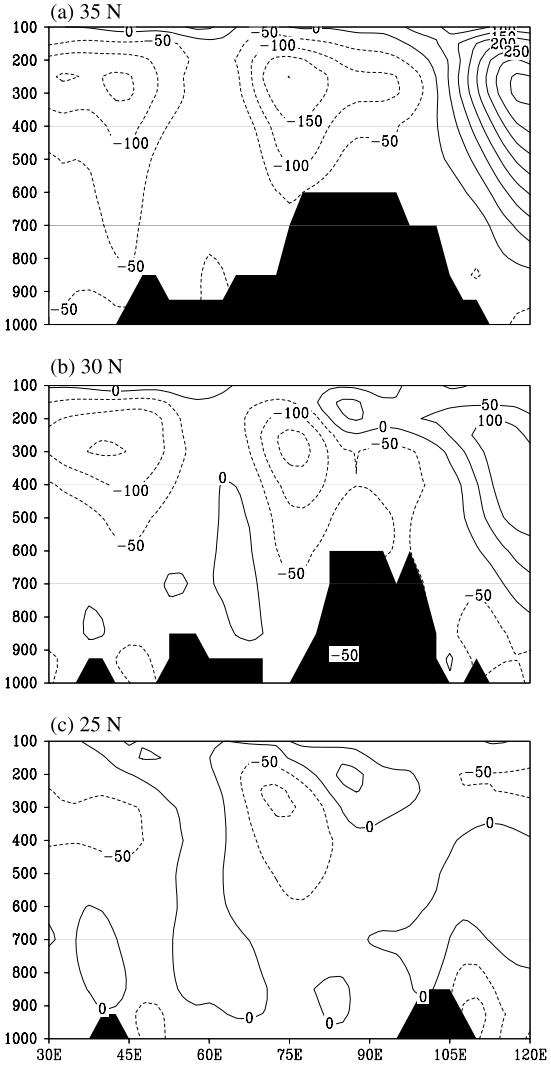

ture is seen at and around the surface. The interaction of orography is demonstrated in the distribution of the moisture field.

3.4.2 Eddy motion ($\overline{v'q'}$)

Vertically integrated seasonal transport of moisture due to eddy motion at 700 hPa, 500 hPa and 300 hPa is shown in Fig. 18. From Fig. 18a, it can be seen that eddy transport at 700 hPa is mainly northwards with higher magnitude over the Red Sea and Saudi Arabia. Significant northward transport of moisture due to eddy motion is also seen over Afghanistan, Pakistan, the Indian Peninsula and the Bay of Bengal. The distribution of meridional transport of moisture due to eddy motion is orientated along the Himalayas, clearly demonstrating the effect of topography. This indicates the fact that due to the interaction of topography and WDs, flowing in the westerlies, most winter precipitation occurs across the region of study. Also, eddy transports higher moisture into the middle and upper troposphere. In particular, it is seen that moving from the lower (700 hPa) to the upper troposphere (300 hPa) the contribution of moisture increases from the Arabian Sea to the Indian Peninsula. At 700 hPa

Fig. 15. Same as Fig. 5, but for meridional transport of potential energy due to eddy motion (units: $m^2\,s^{-1}$)

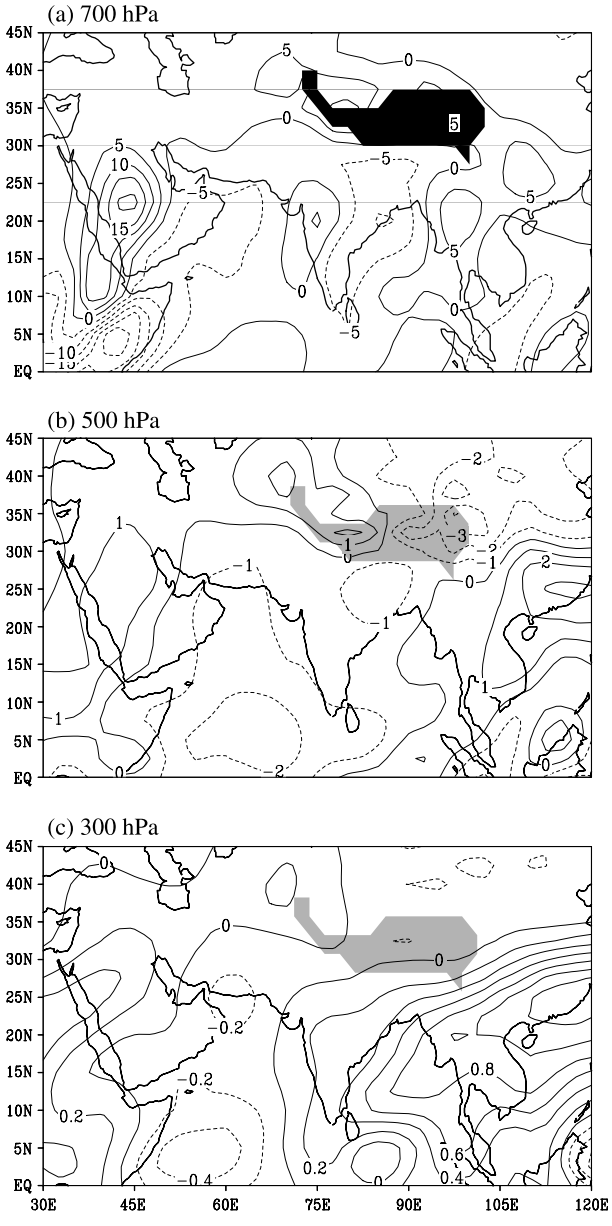

Fig. 16. Same as Fig. 4, but for meridional transport of moisture due to mean motion (units: $\mathrm{kg\,m^{-2}\,s^{-1}}$)

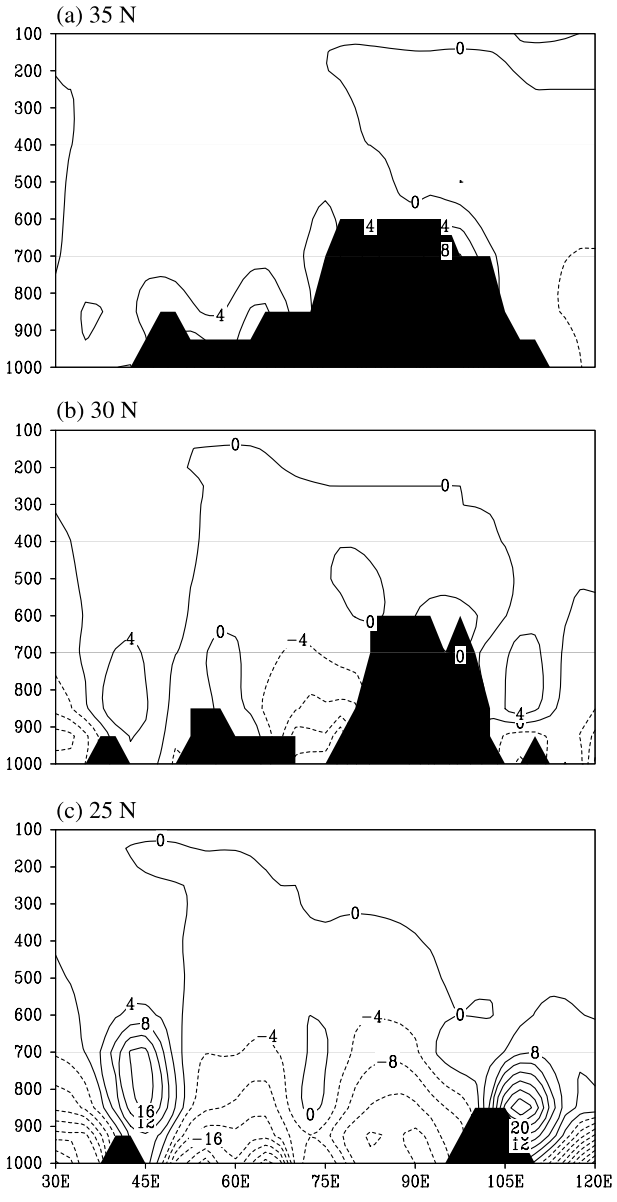

Fig. 17. Same as Fig. 5, but for meridional transport of moisture due to mean motion (units: $\mathrm{kg\,m^{-2}\,s^{-1}}$)

and 500 hPa a strong cell of northward transport of moisture is seen over the Bay of Bengal. Ultimately this moisture is incorporated into the circulations in the westerlies and results in large amounts of winter precipitation over the Himalayan region. In addition to this, the northward contribution of meridional transport of moisture due to eddy motion is greater than the contribution due to mean motion.

Figure 19 shows the sectorial pressure longitude meridional transport of moisture due to eddy motion at 25° N, 30° N and 35° N. Figure 19 indicates that eddy motion mainly contributes towards the northward transport of moisture up to the middle troposphere. The magnitude of the northward transport of moisture due to eddy motion decreases with higher latitude. This strong magnitude of northward transport of moisture due to eddy motion is seen around 45° E and 110° E at all latitudes, with magnitude decreasing from 25° N to 35° N. Here we can also see that eddy motion is more pronounced, and meridional transport of moisture due to eddy motion is greater than due to mean motion.

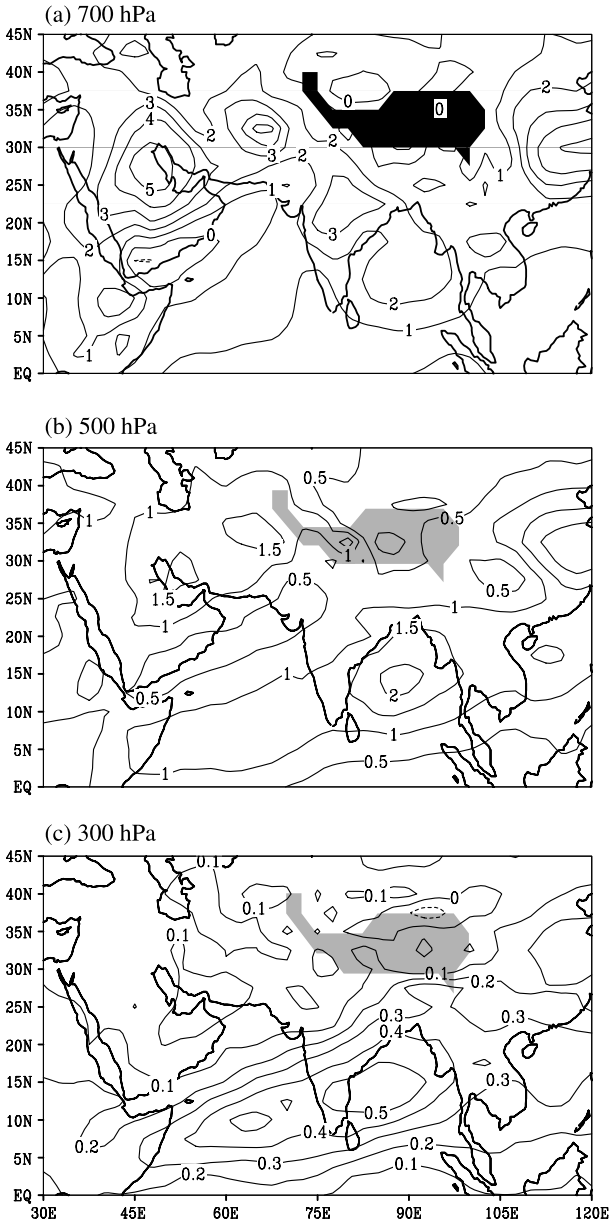

Fig. 18. Same as Fig. 4, but for meridional transport of moisture due to eddy motion (units: $\mathrm{kg\,m^{-2}\,s^{-1}}$)

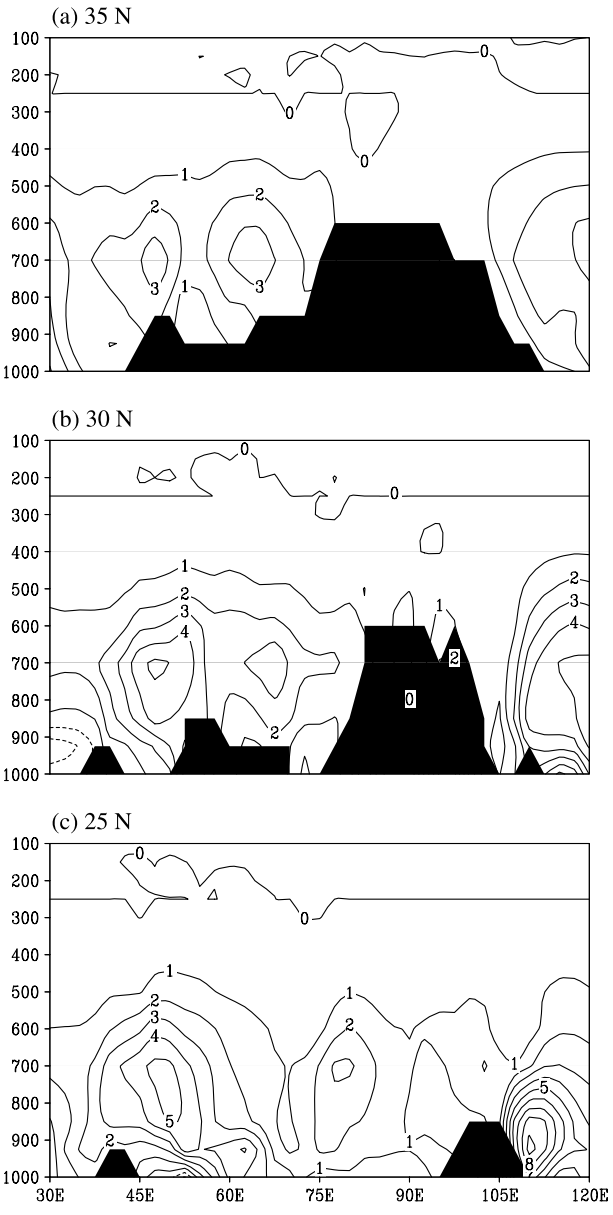

Fig. 19. Same as Fig. 5, but for meridional transport of moisture due to mean motion (units: $\mathrm{kg\,m^{-2}\,s^{-1}}$)

4. Conclusion

The transport of momentum, sensible heat, potential energy and moisture fields show interesting patterns. Most of the fields contribute to northward transport which becomes incorporated into circulation features of WDs embedded in the westerlies and hence result in enormous amount of precipitation. Some of the salient findings of the study are given below.

- The eddy transport of momentum over the western Himalayas is higher than that found in the east in the lower and middle troposphere, whereas the reverse is seen aloft.
- The northward transport of potential energy over the Indian subcontinent leads to the occurrence of the greatest precipitation by amassing moisture from the Arabian Sea over the Indian Himalayan region. This potential energy becomes associated with WDs embedded in the westerly flow and hence yields large amounts of precipitation.
- It is seen that eddy motion contributes more to the meridional transport of moisture than mean motion. Ultimately, this moisture is incorporat-

ed into the circulations in the westerlies and yield large amounts of winter precipitation over the Himalayan region. In addition to this, the northward contribution of meridional transport of moisture due to eddy motion is greater than the contribution due to mean motion.

Overall, these findings can be attributed to the fact that during the passage of WDs, the complex topography of the western Himalayas modifies the westerly flow around 30° N by generating more northward eddy transports.

Acknowledgements

The author acknowledges the National Center for Environmental Prediction (NCEP), US for providing valuable data sets for accomplishing this work. Also, author acknowledges Petra Naschenweng for providing help in figures. Author is very grateful to Prof. Grassl for his approach towards the present work which helped the author in strengthening the paper.

References

Annamalai H, Slingo JM, Sperber KR, Hodges K (1999) The mean evolution and variability of the Asian summer monsoon: comparison of ECMWF and NCEP-NCAR reanalyses. Mon Wea Rev 127: 1157–1186

Chen SC, Norries CL, Roads JO (1996) Balancing the atmospheric hydrologic budget. J Geophys Res 101(D3): 7341–7358

Dimri AP (2005) The contrasting features of winter circulation during surplus and deficient precipitation over Western Himalayas. PAGEOPH 162(2005): 2215–2237, doi: 10.1007/s00024-005-2709-4

Dimri AP (2006) Surface and upper air fields during extreme winter precipitation over Western Himalayas. PAGEOPH 163(2006): 1679–1698, doi: 10.1007/s00024-006-0092-4

Joseph PV (1975) A triennial oscillation of upper tropospheric westerlies and the Indian summer monsoon. Report No. 223, India Meteorology Department, New Delhi, 1–15

Kalnay E et al (1996) The NCEP/NCAR 40 year reanalysis project. Bull Amer Meteor Soc Vol 77: 437–471

Kanamitsu M, Krishnamurti TN (1978) Northern summer tropical circulation during drought and normal rainfall months. Mon Wea Rev 10: 331–347

Krishnamurti TN, Bedi HS, Subramaniam M (1989) The summer monsoon of 1987. J Climate 24: 321–330

Krishnamurti TN, Bedi HS, Subramaniam M (1990) The summer monsoon of 1988. Meteorol Atmos Phys 42: 19–37

Krishnamurti TN, Sinha MC, Nha B, Mohanty UC (1998) A study of south Asian monsoon energetics. J Atmos Sci 55: 2530–2548

Krueger AF, Winston JS (1975) Large scale circulation anomalies over the tropics during 1971–72. Mon Wea Rev 103: 465–473

Kung EC, Smith PJ (1974) Problems of large scale kinetic energy balance, a diagnostic analysis in GARP. Bull Amer Meteor Soc 55: 768–777

Pearce RP (1979) On the concept of available potential energy. Quart J Roy Meteor Soc 104: 737–755

Ramesh Kumar MR, Shenoi SSC, Schluessel P (1999) On the role of the cross equatorial flow on summer monsoon rainfall over India using NCEP/NCAR reanalysis data. Meteorol Atmos Phys 70: 201–213

Sperber KR, Slingo JM, Annamalai H (2000) Predictability and the relationship between subseasonal and interannual variability during the Asian summer monsoon. Quart J Roy Meteor Soc 126: 2545–2574

Starr VP, White RM (1951) A hemispherical study of the atmospheric angular momentum balance. Quart J Roy Meteor Soc 77: 215–225

Author's address: Dr. A. P. Dimri (e-mail: apdimri@hotmail.com, apdimri@yahoo.com), Research and Development Centre, Snow and Avalanche Study Establishment, Him Parisar, Sector 37A, Chandigarh 160036, India.